

# Modification and Stability of Aromatic Self-Assembled Monolayers upon Irradiation with Energetic Particles

P. Cyganik,<sup>\*,†,||</sup> E. Vandeweert,<sup>‡</sup> Z. Postawa,<sup>†</sup> J. Bastiaansen,<sup>‡</sup> F. Vervaecke,<sup>‡</sup> P. Lievens,<sup>‡</sup> R. E. Silverans,<sup>‡</sup> and N. Winograd<sup>§</sup>

Smoluchowski Institute of Physics, Jagiellonian University, ul. Reymonta 4, PL 30-059 Kraków, Poland, Laboratorium voor Vaste-Stoffysica en Magnetisme, Katholieke Universiteit Leuven, Celestijnenlaan 200 D, B-3001 Leuven, Belgium, Department of Chemistry, The Pennsylvania State University, University Park, Pennsylvania 16802, and Institut für Physikalische Chemie 1, Ruhr-Universität Bochum, Universitätsstrasse 150, D-44801 Bochum, Germany

Received: May 20, 2004; In Final Form: November 9, 2004

We have studied ion and electron irradiation of self-assembled monolayers (SAMs) of 2-(4'-methyl-biphenyl-4yl)-ethanethiol (BP2,  $\text{CH}_3\text{-C}_6\text{H}_4\text{C}_6\text{H}_4\text{CH}_2\text{CH}_2\text{-SH}$ ), phenyl mercaptan (PEM,  $\text{C}_6\text{H}_5\text{CH}_2\text{CH}_2\text{-SH}$ ), and 4'-methyl-biphenyl-4-thiol (BP0,  $\text{CH}_3\text{-C}_6\text{H}_4\text{C}_6\text{H}_4\text{-SH}$ ) deposited on Au(111) substrates. Desorption of neutral particles from PEM/Au and BP2/Au was investigated using laser ionization in combination with mass spectrometry. The ion-induced damage of both BP2 and PEM SAMs is very efficient and interaction with a single ion leads to the modification of tens of molecules. This feature is the result of a desorption process caused by a chemical reaction initiated by an ion impact. Both for ions and electrons, experiments indicate that the possibility for scission of the Au-S bond strongly depends on the chemical nature of the SAM system. We attribute the possible origin of this effect to the orientation of the Au-S-C angle or adsorption sites of molecules. The analysis of electron-irradiated PEM/Au and BP2/Au, using ion-initiated laser probing, enabled measurements of the cross section for the electron-induced damage of the intact molecule or specific fragment. Analysis of electron-irradiated BP0/Au by using time-of-flight secondary ion mass spectrometry (TOF-SIMS) provides *direct* evidence for the quasi-polymerization process induced by electron irradiation.

## I. Introduction

Self-assembled monolayers (SAMs) are organic molecular assemblies that spontaneously form dense and ordered monolayers on appropriate substrates.<sup>1</sup> These monolayers have been successfully deposited on metals such as gold, silver, copper, platinum, and chromium<sup>2–5</sup> and on oxide and semiconductor surfaces such as  $\text{SiO}_2$  and GaAs.<sup>1–7</sup> Depending upon the molecular design, SAMs provide a way to tailor surface properties such as wetting,<sup>8</sup> friction,<sup>9</sup> and corrosion.<sup>10</sup> The high attraction of SAMs is also driven by the simple preparation procedure, the reproducible film quality, and stability of a monolayer. Therefore, SAMs are presently very interesting for scientists in such diverse disciplines as physics, chemistry, and biology.<sup>1</sup> So far, most of the fundamental studies have been performed with alkane thiols.<sup>1</sup> More recently, aromatic thiols, that is, thiol-based SAMs including an aromatic moiety, are of interest because of their potential applications in molecular electronics.<sup>11–19</sup>

With respect to these applications, the response of these monolayers to electron and ion irradiation, key device processing tools, is largely lacking. Because of the small dimensions associated with these molecular systems, such as an intermolecular distance of less than 1 nm and a typical thickness of about 2 nm, the potentially attainable resolution in electron and ion lithography of SAMs is very high. This property has already

been demonstrated with electrons,<sup>20,21</sup> ions,<sup>22</sup> and photons.<sup>23</sup> In electron lithography, sub-10 nm resolution was achieved.<sup>20</sup> Furthermore, Götzhäuser et al. demonstrated the fabrication of gold nanostructures by electron beam patterning and subsequent wet etching of a gold substrate covered by SAMs based on thiols.<sup>24</sup> These experiments showed that alkane and aromatic thiols can be applied as positive and negative electron beam resists, respectively. However, a significantly higher quality of the pattern transfer was achieved in the aromatic thiols. Recently, electron beam lithography of aromatic thiols was utilized to produce a spatially selective electrochemical passivation and thus allowed electrochemical deposition of a copper pattern.<sup>25</sup>

For electron and ion lithography, further improvements in the resist properties of SAMs, such as contrast, sensitivity, and defect density, depend crucially on the understanding of the beam damage mechanisms. Up to now, these mechanisms have been obtained by analysis of the compositional or structural changes in pristine SAMs *after* irradiation.<sup>26–35</sup> There are only a few measurements that focus on the investigation of the fragments emitted from these systems *during* irradiation. This type of study provides information concerning ion<sup>36–38</sup> and electron<sup>39–41</sup> induced desorption mechanisms from SAM films.

Previously, we investigated ion-stimulated desorption of neutral molecules emitted from 8 keV  $\text{Ar}^+$  ion-bombarded SAMs of 2-(4'-methyl-biphenyl-4yl)-ethanethiol (BP2,  $\text{CH}_3\text{-C}_6\text{H}_4\text{C}_6\text{H}_4\text{CH}_2\text{CH}_2\text{-SH}$ )<sup>38</sup> and phenylethyl mercaptan (PEM,  $\text{C}_6\text{H}_5\text{CH}_2\text{CH}_2\text{-SH}$ ).<sup>36,37</sup> The results obtained in these measurements showed that most of the neutral molecules are emitted with low (thermal) energies. In the proposed model, low-energy desorption of neutral molecules was viewed as a two-step

\* Corresponding author e-mail: cyganik@pc.ruhr-uni-bochum.de.

† Jagiellonian University.

‡ Katholieke Universiteit Leuven.

§ The Pennsylvania State University.

|| Ruhr-Universität Bochum.

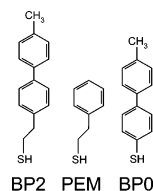


**Figure 1.** Schematic drawing of the molecules BP2, PEM, and BP0 used in this study.

process.<sup>36</sup> In the first step, the impact of the projectile initiates both chemical and physical processes (e.g., reactions and the generation of secondary electrons) that gently fragment surface-bound molecules. The created fragments remain physisorbed on the surface until they evaporate. The emission of the molecular fragments was dependent on the surface temperature<sup>36,37</sup> and on the mass of the emitted fragment.<sup>38</sup> Only a small fraction of the molecules is emitted with hyperthermal kinetic energies (about 2–3 eV). In this case, emission was attributed to the direct collisions between a projectile and ejected substrate particles.

Recently, we demonstrated that sensitive laser probing of desorbed species can be exploited to study in situ the processes that occur during interaction of organic SAMs with low-energy electrons.<sup>41</sup> These experiments provide direct evidence that energetic electrons can induce desorption of large, fragile neutral molecular fragments. In this paper, both ion and electron desorption experiments for BP2/Au(111) and PEM/Au(111) systems are compared. The BP2 and PEM molecules selected for this study are similar in chemical composition but form films of different structure. Hence, it is possible to determine how the arrangement of the molecules in the monolayer influences the desorption process. Another aspect of this study is the in-situ evaluation of the damage as a function of accumulated fluence. In electron irradiation, the cross section for modification of the intact molecule and certain molecular fragments is presented. Finally, to understand the general character of structure modification in aromatic SAMs induced by electron irradiation, an ex-situ TOF–SIMS analysis of model aromatic systems of 4'-methyl-biphenyl-4-thiol (BP0,  $\text{CH}_3\text{-C}_6\text{H}_4\text{C}_6\text{H}_4\text{-SH}$ ) is performed. These results directly reveal a modification mechanism which makes aromatic SAMs useful as a positive electron beam resist and which has up to now been assumed by others from indirect observations.

## II. Experimental Section

**Sample Preparation.** 2-(4'-Methyl-biphenyl-4-yl)ethanethiol (BP2)  $\text{CH}_3\text{-C}_6\text{H}_4\text{C}_6\text{H}_4\text{CH}_2\text{CH}_2\text{-SH}$ , phenylethyl mercaptan (PEM)  $\text{C}_6\text{H}_5\text{CH}_2\text{CH}_2\text{-SH}$ , and 4'-methyl-biphenyl-4-thiol (BP0)  $\text{CH}_3\text{-C}_6\text{H}_4\text{C}_6\text{H}_4\text{-SH}$  monolayers were prepared by (24 h) immersion of 200-nm-thick polycrystalline gold films evaporated on freshly cleaved mica substrates<sup>42</sup> in ethanolic 1 mM thiol solutions (see Figure 1 for schematic drawing of molecules). PEM was obtained from Aldrich. BP2 and BP0 molecules were synthesized at the University of Heidelberg by a procedure described elsewhere.<sup>43</sup> After removal from the solution, all samples were rinsed with ethanol and dried in a nitrogen stream.

**Ion Irradiation Experiments.** Five hundred nanosecond pulses of 15 keV  $\text{Ar}^+$  ions focused onto a 3-mm spot on the sample were used to stimulate desorption of molecules and molecular fragments. Desorbed neutral molecules were detected by a laser-ionization mass spectrometer. The experimental setup is described in detail elsewhere.<sup>44</sup> In short, the apparatus consists of an ultrahigh vacuum chamber (base pressure below  $2 \times 10^{-10}$

hPa) in which an ion and an electron gun were used to direct energetic projectiles at  $45^\circ$  incidence onto a centrally located sample. The plume of desorbed particles was intersected (parallel to the sample surface at a distance of 4 mm) by a focused laser beam from a pulsed (10 Hz repetition frequency) Nd:YAG pumped optical parametric oscillator delivering 6 ns pulses (3 mJ/pulse). Desorbed organic fragments were ionized using laser radiation at 259 nm with a fluence of  $7.3 \times 10^{17}$  photons/cm<sup>2</sup>. At this wavelength, a large photoion yield was observed, attributed to the resonance-enhanced two-photon ionization as was reported for benzene molecules.<sup>45</sup> The photoions were subsequently detected by a time-of-flight (TOF) mass spectrometer with a mass resolution  $m/\Delta m$  of about 800 in the reflectron mode in the range of  $m/z$  below 200. For weak signals, a linear mode spectrometer was used ( $m/\Delta m = 200$  at  $m/z$  in the range of 200). All measurements were made under static conditions with the total ion fluence kept below  $10^{11}$  ions/cm<sup>2</sup>.

**Electron Irradiation Experiments.** The experiments were performed in the same experimental system as the ion irradiation experiments. Electron-induced damage was investigated by using a 150 eV electron beam. During the irradiation sessions, the electron beam was scanned with TV frequency over an area of  $1.5 \times 1.5$  cm<sup>2</sup>. The electron flux during the irradiation experiments was  $3 \times 10^{12}$  electrons/cm<sup>2</sup> s ( $0.48 \mu\text{A}/\text{cm}^2$ ). Desorption mass spectra were obtained in the linear mode of the mass spectrometer with the energy of the electron beam being 1 keV. Although initially the intention was to keep the kinetic energies of the electrons as low as possible, they were not a central issue at this point and their values are dictated by technical considerations. At low energies, the focusing capacity of the electron gun deteriorates and thus with a constant acceptance angle to the mass spectrometer and (most likely) a lower yield, much smaller signals were obtained when desorbing with 150 eV compared to 1 keV. The electron flux in this case was  $4 \times 10^{12}$  electrons/cm<sup>2</sup> s ( $0.64 \mu\text{A}/\text{cm}^2$ ) and the total electron fluence delivered during the entire measurement (50 s) was about  $32 \mu\text{C}/\text{cm}^2$  ( $2 \times 10^{14}$  electrons/cm<sup>2</sup>).

**SIMS Analysis of Electron-Irradiated Samples.** Secondary ion mass spectra were obtained in a dedicated TOF–SIMS mass spectrometer operated at a base pressure below  $2 \times 10^{-10}$  hPa. This system is described in detail elsewhere.<sup>46</sup> Briefly, ion-stimulated desorption was initiated by 25 keV, 35-ns pulses of a  $\text{Ga}^+$  ion beam at a repetition rate of 3 kHz. During the measurements, the ion beam (with an ion current of 2 nA for a continuous beam) scanned an area of  $500 \times 500 \mu\text{m}$  and the mass spectra were recorded with mass resolution  $m/\Delta m$  of about 1000 and 1700 for  $m/z$  in the range of 200 and 600, respectively. All TOF–SIMS measurements were performed under static conditions where the total ion fluence was kept below  $10^{11}$  ions/cm<sup>2</sup>. The electron irradiation of the samples was performed ex situ using the same system as for other electron experiments.

## III. Results

**Photoionization Experiments for Gas-Phase BP2 and PEM.** Photoionization of molecules by irradiation of ns-laser light is a powerful tool to bring neutral particles into a charged, that is, detectable state. As the ionization energies of many molecules are about 5 eV or more, most often two or more photons need to be absorbed before the molecule can be excited into the ionization continuum. By operating a tunable laser system at a wavelength matching the energy difference needed for an electronic transition, the overall efficiency of the ionization scheme can be dramatically enhanced. However, complex molecules are also prone to photodissociation before

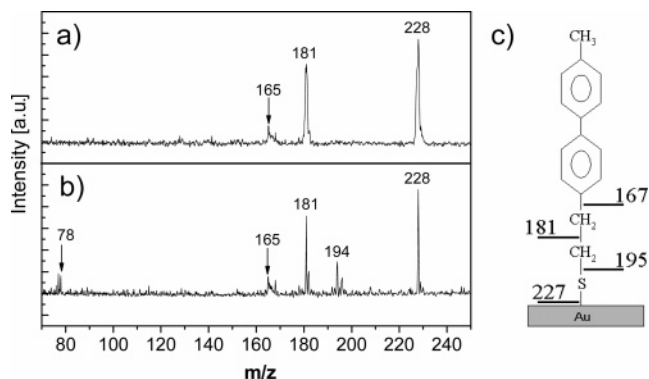


**Figure 2.** Mass spectra of neutral molecules obtained upon photoionization of (a) BP2 molecules in the gas-phase above Au substrate and (b) molecules desorbed from BP2/Au during bombardment by 15 keV  $\text{Ar}^+$  ions. A schematic drawing of the BP2 molecule on Au substrate with an indication of the masses of the fragments resulting from breaking selected C–C bonds is shown in panel c.

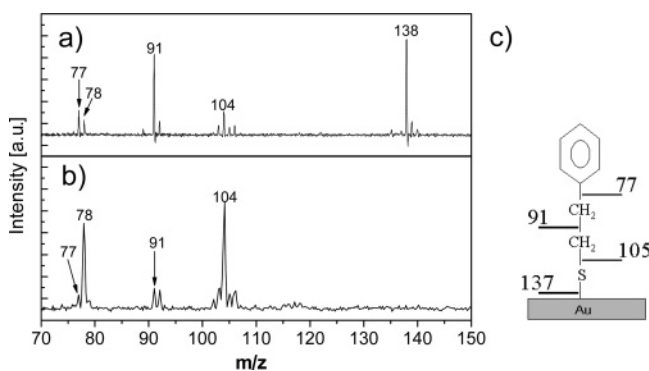


**Figure 3.** Mass spectra of neutral molecules obtained upon photoionization of (a) PEM molecules in the gas-phase above Au substrate and (b) molecules desorbed from PEM/Au during bombardment by 15 keV  $\text{Ar}^+$  ions. A schematic drawing of the PEM molecule on Au substrate with an indication of the masses of the fragments resulting from breaking selected C–C bonds is shown in panel c.

the complete molecule can be photoionized. The resulting fragmentation patterns can be very complex and critically depend on the wavelength and intensity of the laser light. Prior to experiments on particle-irradiated SAMs, we investigated the photoionization behavior of BP2 and PEM molecules in the gas phase. At room temperature, PEM is in the liquid state and can be easily brought into the gas phase at sufficiently high vapor pressures in the vacuum chamber (typ.  $10^{-9}$  hPa). On the contrary, BP2 is solid at room temperature and has to be solvated. To detect gas-phase BP2 molecules, a SAM was inserted in the apparatus without undergoing a thorough rinsing-and-drying procedure. Such a sample contains both chemisorbed molecules forming the SAM and molecules loosely entangled in the monolayer. These physisorbed molecules evaporate after insertion in the vacuum system and their vapor pressure was high enough for detection of gas-phase molecules.

The measured mass distributions after ionization of gas-phase BP2 and PEM together with a schematic representation of both molecules are shown in Figure 2 and Figure 3, respectively. The mass spectrum obtained for gas-phase BP2 molecules (Figure 2a) exhibits groups of peaks around  $m/z$  of 165, 181, and 228. The mass 228 corresponds to the mass of the complete BP2-molecule ( $m/z = 228$ ,  $\text{CH}_3\text{-C}_6\text{H}_4\text{C}_6\text{H}_4\text{CH}_2\text{CH}_2\text{-SH}$ ). The other fragments result from breaking of C–C bonds in the alkane chain (see schematic drawing of BP2 molecule in Figure 2c). Their abundance is strongly dependent upon the photon fluence, and thus they are considered as products of the

photofragmentation of the complete molecule. For the gas-phase PEM molecules (Figure 3a), it is also possible to detect the intact molecule ( $m/z = 138$ ,  $\text{C}_6\text{H}_5\text{CH}_2\text{CH}_2\text{-SH}$ ). In this case, photofragmentation predominantly leads to the formation of fragments at  $m/z = 91$ . The intensity of other fragments with  $m/z$  values of 78 and 104 is much lower. These measurements clearly show that the employed laser ionization system is capable of detecting complete molecules for both SAMs. Although the same wavelength of the post-ionization laser system was employed in earlier studies, complete molecules for both BP2<sup>38</sup> and PEM<sup>37</sup> could not be detected. We attribute this difference to the higher photon density used in the previous studies.

**Ion-Stimulated Desorption of BP2 and PEM.** For these experiments, the preparation procedure of BP2 and PEM samples described in section 2 was followed, and special care was taken to remove all physisorbed remnants before the data acquisition. As a result, within the instrumental detection limit no gas-phase species could be detected for either monolayer before ion irradiation.

The mass spectrum recorded during ion irradiation of a BP2 monolayer with 15 keV  $\text{Ar}^+$  is shown in Figure 2b. As for the gas-phase spectrum, the emission of the intact molecule is observed.<sup>47</sup> However, in addition to the peaks observed in the gas-phase experiment (Figure 2a), molecular fragments, with  $m/z$ -values centered around 78 and 194, are also present.

A different behavior is observed for the PEM system (Figure 3b). In contrast to data obtained upon irradiation of BP2 (Figure 2b), the parent molecule is not present in the mass spectrum obtained during ion irradiation of the PEM monolayer, although as it was shown in the previous section, the laser system is capable of detecting the molecule in the gas phase. Consequently, the intact molecule is not ejected from an  $\text{Ar}^+$  irradiated PEM/Au monolayer. In addition, the relative intensities of the fragments near  $m/z = 78$  and 104 are significantly higher than the intensity of the fragment detected at  $m/z = 91$ . This observation is opposite to that obtained in the gas-phase experiment. The low intensity of fragments at  $m/z = 78$  and 104 for PEM and lack of fragments at  $m/z = 78$  and 194 for BP2 in the respective gas-phase spectra could indicate that these fragments are directly emitted from the monolayer after ion impact. During sputtering, the molecule can gain internal energy, so that its photofragmentation behavior may not be the same as for a gas-phase molecule examined at room temperature. A comparison of the ion-induced spectra with gas-phase spectra cannot strictly rule out that the fragments emitted from PEM and BP2 monolayers at  $m/z = 78$ , 104, and 194 are an effect of photofragmentation of an excited parent molecule. However, the data presented in the next section show that the cross sections for electron-induced damage obtained for these fragments depend on the fragment mass. Since these cross sections are measured as changes in the mass spectra obtained by ion sputtering between consecutive electron irradiation sessions, the observed mass dependence can only be explained if these analyzed fragments are directly emitted from the surface. Moreover, we previously reported that the flight-time distributions of the individual molecular fragments detected upon ion bombardment of both PEM and BP2 SAMs are markedly different.<sup>38</sup> In case all fragments in the mass spectra would stem from the photofragmentation of the parent molecule, their flight-time distributions should be the same. Since this is not the case, we conclude that photodissociation of desorbed parent molecules can be neglected.

To estimate the sensitivity to degradation resulting from ion irradiation of BP2 and PEM monolayers, changes in the signal

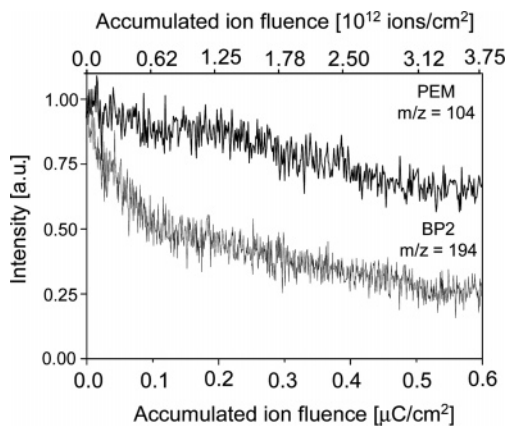


**Figure 4.** Photoion signal from the desulfurized molecular fragments of  $m/z = 194$  and  $m/z = 104$  as a function of the accumulated ion fluence during bombardment of BP2/Au and PEM/Au by 15 keV  $\text{Ar}^+$  ions, respectively.

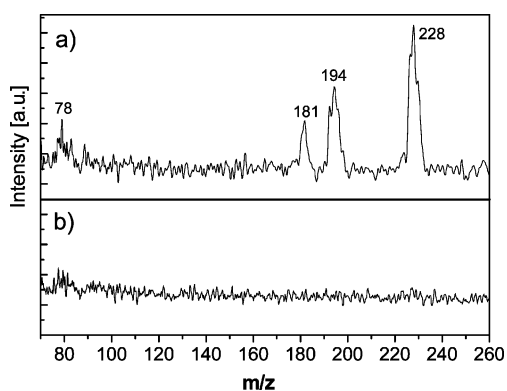


**Figure 5.** (a) Mass spectrum of neutral molecules obtained upon photoionization of molecules desorbed from BP2/Au during irradiation by 1 keV electrons. The background signal recorded in the same experiment with the electron beam turned off is shown in panel b.

of the respective fragments at  $m/z = 194$  and 104 were monitored as function of the ion irradiation fluence (Figure 4). For SAMs, static conditions are usually assumed when the total fluence of bombarding ions is kept below  $5\text{--}10 \times 10^{12}$  ions/ $\text{cm}^2$ .<sup>48–50</sup> Monitoring the neutral channels of ion-induced desorption indicates that BP2 and PEM monolayers already undergo significant modification at a much lower fluence of  $3.7 \times 10^{12}$  ions/ $\text{cm}^2$  ( $0.6 \mu\text{C}/\text{cm}^2$ ). In addition, this modification is more efficient for BP2 than for the PEM monolayer. This observation is in agreement with the expectation that the damage cross section should increase with the size of the molecule and that desorption of the intact molecule is observed only for BP2. Both of these observations indicate that there is a lower stability of this monolayer toward ion irradiation.

**Electron-Stimulated Desorption of BP2 and PEM Monolayers.** In this section, two kinds of experiments are conducted. In the first experiment, the desorption of BP2 and PEM monolayers induced by a 1 keV electron beam are investigated. In the second experiment, the electron-induced damage in the SAM was monitored in situ as a function of the accumulated fluence.

In general, the photoion signals are considerably smaller than those acquired during the ion-induced desorption experiments because of the lower electron current (see Figure 5 and 6). To improve the signal-to-noise ratio, the mass spectrometer was operated in the linear mode, resulting in a substantially higher transmission through the instrument but at the cost of a reduced mass resolution. The result presented in Figure 5a for the BP2

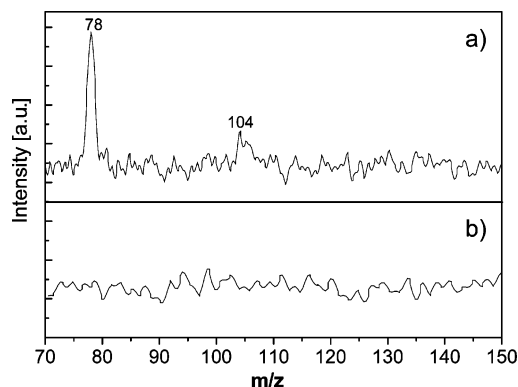


**Figure 6.** (a) Mass spectrum of neutral molecules obtained upon photoionization of molecules desorbed from PEM/Au during irradiation by 1 keV electrons. The background signal recorded in the same experiment with the electron beam turned off is shown in panel b.

system provides direct evidence that medium-energy electrons are capable of initiating the desorption of large neutral molecular fragments from the organic overlayer. It is evident that both the intact molecule ( $m/z = 228$ ) and the desulfurized fragment ( $m/z = 194$ ) are ejected.

The mass spectrum of the electron-desorbed PEM system is shown in Figure 6a. In this case, the emission of the complete molecule is not observed and the ejection of the desulfurized fragment is very weak. To prove that the observed emission from BP2 and PEM monolayers is directly stimulated by the electron-induced desorption process, the background mass spectra obtained during the experiment when the electron beam is turned off are also presented in Figure 5b and Figure 6b, respectively.

To monitor electron-induced damage, pristine SAMs made of BP2 and of PEM molecules were uniformly exposed to a 150 eV beam during consecutive sessions. Between two sessions, we could assess the damage induced in the BP2 and PEM monolayers by electron irradiation using ion-initiated laser probing. The ion fluence per data point was kept as low as  $1.3 \times 10^{10}$  ions/ $\text{cm}^2$  ( $2 \text{ nC}/\text{cm}^2$ ) to keep the ion-induced damage in the “effective” static range according to the results presented above. Ion- and electron-induced damage was considered to be uncorrelated and the data are corrected for ion-initiated degradation, which was about a few percent. For the BP2 monolayer, the decrease of the photoion signal from the intact molecule ( $m/z = 228$ ) and the desulfurized fragment characterized by  $m/z = 194$  peak as a function of the accumulated fluence is presented in Figure 7. The corresponding data obtained for fragments  $m/z = 78$  and 104 ejected from PEM samples are shown in Figure 8.

**SIMS Analysis of Electron-Induced Damage in BP0.** In previous XPS, NEXAFS, and IR investigations of the electron-induced modification in SAMs, it has been demonstrated that in contrast to alkanethiols,<sup>26–28,31,34</sup> even after a high ( $\sim 10^4 \mu\text{C}/\text{cm}^2$ ) electron fluence, aromatic SAMs are only partially disordered and remain bound to the gold substrate.<sup>24,32,35</sup> Although the latter conclusion is not strictly valid as was shown in section 3.3, the former is supported by recent etching experiments.<sup>24,32</sup> These experiments demonstrate that electron irradiation of  $\text{C}_6\text{H}_5\text{C}_6\text{H}_4\text{--SH}$  based SAMs with fluences in the range of  $10^4 \mu\text{C}/\text{cm}^2$  induces an increased chemical etching resistance (in KCN/KOH solution), and therefore these materials behave as a negative resist. An increase in the chemical resistance and the changes observed in the infrared spectra provide indirect evidence of cross-linking between neighboring phenyl groups, resulting in a quasi-polymerization. The manifestation of this

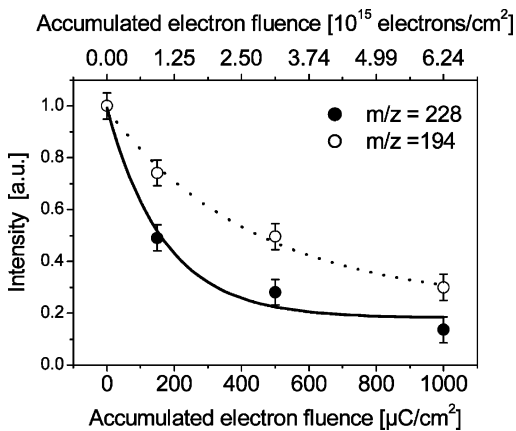


**Figure 7.** Photoion signals from the thiolate ( $m/z = 228$ ) and desulfurized molecular fragment ( $m/z = 194$ ) as a function of the accumulated electron fluence during uniform irradiation of the BP2/Au system by 150 eV electrons. The solid and dotted lines represent decay function (eq 1) for  $m/z = 228$  and  $m/z = 194$  data, respectively.

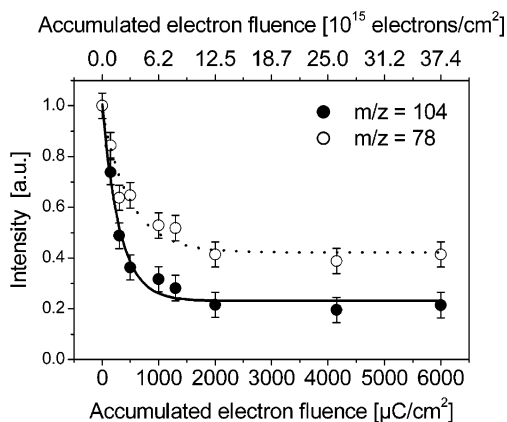


**Figure 8.** Photoion signals from the desulfurized molecular fragment ( $m/z = 104$ ) and another fragment ( $m/z = 78$ ) as a function of the accumulated electron fluence during uniform irradiation of the PEM/Au system by 150 eV electrons. The solid and dotted lines represent decay function (eq 1) for  $m/z = 104$  and  $m/z = 78$  data, respectively.

polymerization is basic for the understanding of the modification process taking place in the aromatic SAMs which is crucial for the potential application of these materials for electron lithography. This type of reaction has not yet been confirmed by any direct experiment.

To investigate this type of electron-induced modification of aromatic SAMs, SIMS experiments from BP0 ( $\text{CH}_3\text{-C}_6\text{H}_4\text{C}_6\text{H}_4\text{-SH}$ ) molecules were performed. This system is very similar to  $\text{C}_6\text{H}_5\text{C}_6\text{H}_4\text{-SH}$  reported earlier,<sup>24,32</sup> where cross-linking is clearly observed. In the present approach, both the changes in the stability and the structure of the irradiated monolayer are investigated. For these purposes, the BP0/Au(111) samples were first irradiated by 150 eV electrons with fluences of 0,  $10^2$ ,  $10^3$ , and  $10^4 \mu\text{C}/\text{cm}^2$  and then exposed to ambient atmosphere for the next 30 days before insertion in the high-resolution TOF-SIMS system. As a reference measurement, TOF-SIMS mass spectra for a pristine BP0 sample analyzed immediately after preparation were also recorded.

In Figure 9, positive and negative SIMS spectra recorded for the pristine BP0 sample are presented. In the negative mass spectra, characteristic ions  $(\text{M-H})^-$ ,  $(\text{Au}_2[\text{M-H}])^-$ , and  $(\text{Au}[\text{M-H}]_2)^-$  are observed, where M corresponds to the complete BP0 molecule, that is,  $\text{CH}_3\text{-C}_6\text{H}_4\text{C}_6\text{H}_4\text{-SH}$ . We are not aware of any SIMS spectra for this kind of aromatic SAMs, but for alkanethiols/Au(111), the emission of secondary ions such as  $(\text{Au}_2[\text{M-H}])^-$  and  $(\text{Au}[\text{M-H}]_2)^-$  is very typical.<sup>49</sup> The emission of the  $(\text{M-H})^-$  quasi-molecular ion has also been reported for alkanethiols; however, it was not so pronounced as it is in BP0. In the positive ion mass spectra, characteristic ions such as  $(\text{M-H})^+$  and  $(\text{Au}[\text{M-H}])^+$  are observed. The latter ion was also observed in the SIMS experiments performed for alkanethiols monolayers, but there is no evidence of the former quasi-molecular ion in this study.<sup>48</sup> In conclusion, in contrast to the alkanethiols monolayers, a pronounced emission of the quasi-molecular secondary ions is observed both in negative and positive SIMS mass spectra of BP0.

In the negative mass spectra taken for samples exposed to air for 30 days (see data in Figure 10k-o), a strong signal from the sulfonate species of  $(\text{SO}_3)^-$  and  $(\text{HSO}_4)^-$  is recorded. These peaks together with characteristic secondary ions observed in the negative spectra ( $(\text{M-H})^-$ ,  $(\text{Au}_2[\text{M-H}])^-$ , and  $(\text{Au}[\text{M-H}]_2)^-$ ) decrease significantly as a function of the total electron fluence (Figure 10a-j). In the corresponding positive mass spectra, a small increase in the intensity of characteristic secondary ions ( $(\text{M-H})^+$ ,  $(\text{Au}[\text{M-H}])^+$ ) up to a fluence of  $10^3 \mu\text{C}/\text{cm}^2$  is observed, followed by the complete disappearance of these peaks after a fluence of  $10^4 \mu\text{C}/\text{cm}^2$  (Figure 11a-j). Additionally, after an electron fluence of  $10^4 \mu\text{C}/\text{cm}^2$ , two pronounced mass peaks at  $m/z = 331$  and  $332$  occur in the mass

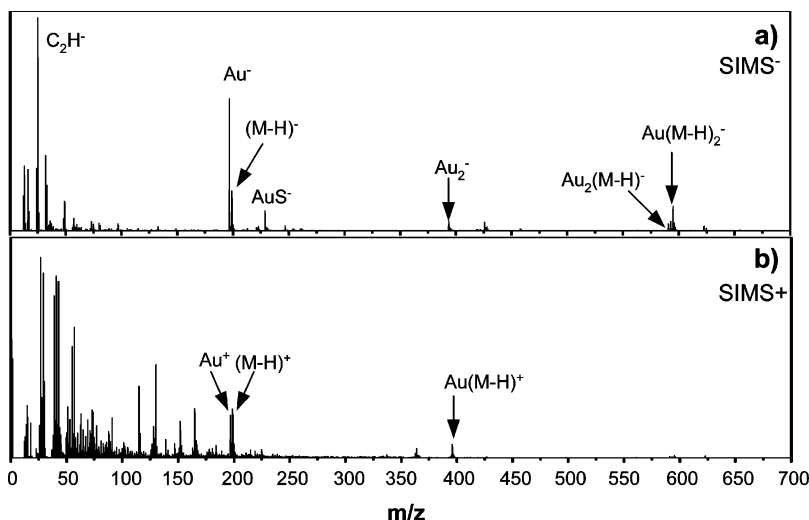


**Figure 9.** (a) Negative and (b) positive SIMS spectra acquired for the pristine BP0/Au system using 25 keV,  $\text{Ga}^+$  ion beam.

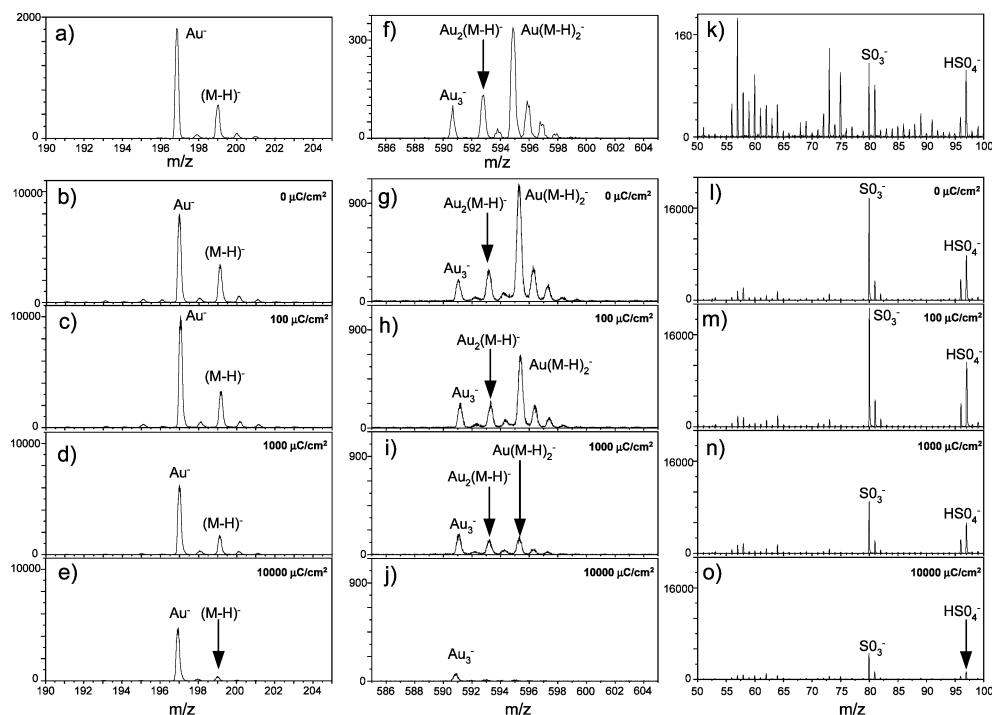


**Figure 10.** Negative SIMS spectra (25 keV,  $\text{Ga}^+$ ) acquired for the pristine BP0/Au system (a, f, and k) and for BP0/Au samples uniformly irradiated by 150 eV electron beam and stored for 30 days in air (b–e, g–j, and l–o). The electron fluence was varied between 0 and 10,000  $\mu\text{C}/\text{cm}^2$ .

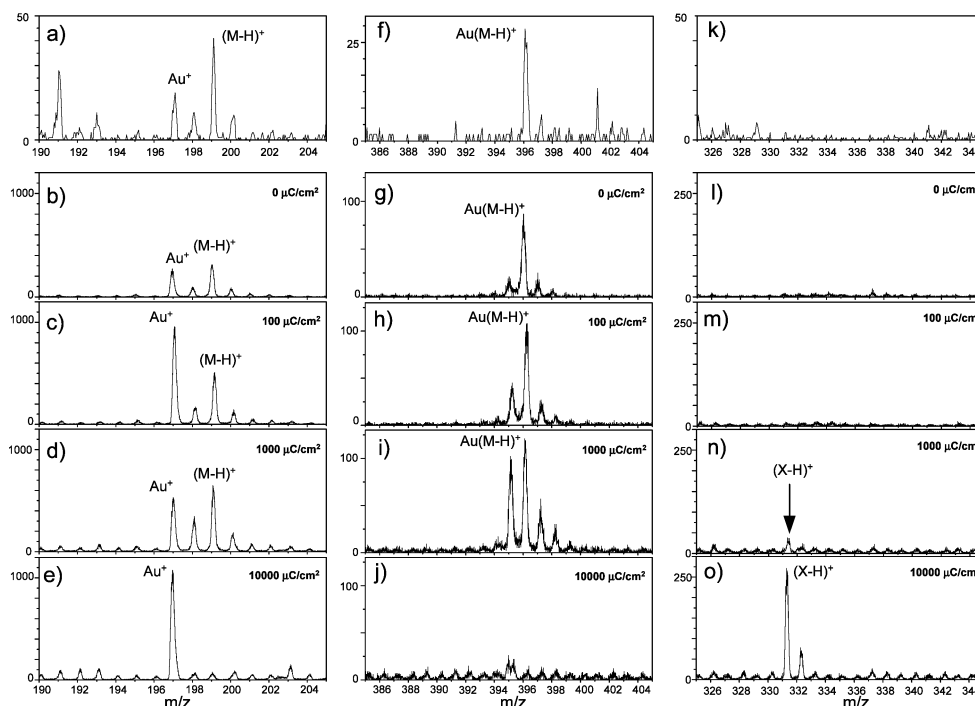


**Figure 11.** Positive SIMS spectra (25 keV,  $\text{Ga}^+$ ) acquired for the pristine BP0/Au system (a, f, and k) and for BP0/Au samples uniformly irradiated by 150 eV electron beam and stored for 30 days in air (b–e, g–j, and l–o). The electron fluence was varied between 0 and 10,000  $\mu\text{C}/\text{cm}^2$ .

spectrum (Figure 11k–o). These peaks are not observed for the reference pristine BP0 sample nor for samples irradiated with fluences below  $10^4 \mu\text{C}/\text{cm}^2$ .

#### IV. Discussion

**Electron Irradiation Experiments.** From the electron desorption experiments presented in Figures 5 and 6, one can conclude that in BP2 monolayers electron-induced processes may lead to the cleavage of both S–C and Au–S bonds and

then to the emission of the desulfurized and complete molecule, respectively. In contrast, results obtained for PEM indicate that cleavage of the S–C and particularly the Au–S bond is very ineffective and will lead to the formation of a sulfur layer. This striking difference in electron-induced cleavage of the S–C and Au–S bonds in BP2 and PEM SAMs is very interesting considering that in both cases aromatic rings are bound to the substrate by two  $\text{CH}_2$  groups and a sulfur atom.

Interaction of electrons with molecules leads to excitation

and ionization processes. Some of these processes will lead to the formation of repulsive states and ultimately to dissociation of the molecule. In SAMs on gold, one has to consider that the proximity of the metal substrate can give rise to nonradiative relaxation of the repulsive state, which will lower the dissociation probability.<sup>51</sup> It has been shown that, for a molecule which is not chemically bound to the metal substrate, nonradiative quenching of the excited state in the proximity of the metal substrate can be described as the interaction between an oscillating dipole and its image. This interaction may lead to the creation of an electron–hole pair or phonon in the metal substrate.<sup>51</sup> For an excited molecule chemically bound to the metal substrate, additional, nonradiative quenching by electron tunneling between the molecule and the metal can occur. For both quenching processes, the relaxation probability will decrease rapidly with the distance between the location of the excitation and the metal substrate. This strong distance dependence of the quenching process is believed to be responsible for inhomogeneous C–H bond scission throughout the alkanethiol monolayers on gold.<sup>27</sup> It is clear that for molecules chemisorbed on a metal substrate, quenching via electron tunneling will strongly depend on the details of the chemical bonding between molecule and substrate, such as the value and orientation of the Au–S–C bond angle or the adsorption site of sulfur on Au(111).

In thiol-based SAMs on gold, usually  $sp^3$  hybridization is assumed for the chemical bonding leading to a Au–S–C bond angle of about  $104^\circ$ .<sup>52,53</sup> In fact, the Au–S–C angle may change substantially because it results from the competition between optimizing substrate–thiolate interaction (including the Au–C–S bending potential) and the intermolecular interaction between the molecules in the film to achieve the energetically most favorable configuration of the system. Thus, the value of the Au–S–C bond angle will depend on the specific system as it was recently concluded by Rong et al.<sup>43</sup> from the spectroscopic investigation of aromatic SAMs on Au(111) where the biphenyl group was separated by an alkane spacer containing  $n$   $CH_2$  units (BP $n$ ,  $n = 1–6$ ). For a biphenyl group separated by an odd number of the  $CH_2$  units, they concluded that the molecules are bound with a Au–S–C bond angle between  $94$  and  $105^\circ$ , which is very close to the value obtained for  $sp^3$  hybridization. However, for an even number of methylene units such as the BP2 molecule, a value of more than  $130^\circ$  was found. This strongly deviates from the  $sp^3$  value.<sup>43</sup> Generally, for BP $n$  systems on gold, a favorable value of Au–S–C angle corresponding to  $sp^3$  hybridization with, at the same time, an optimized coverage and molecular packing can only be accomplished for odd values of  $n$ . For even values of  $n$ , there is a conflict between these two factors resulting in a decrease of the coverage and an increase in the Au–S–C bond angle to accommodate for the tilting of the biphenyl part of the molecule.<sup>43</sup> Since the aromatic part of the PEM molecule is much shorter as compared to BP2, we expect a significant difference in the intermolecular interaction for these two systems and thus in the Au–S–C angle as a result of their mutual interplay.

As mentioned above, the adsorption site of the sulfur atom is another factor influencing the coupling between the sulfur atom and the gold substrate<sup>54</sup> and hence may affect the efficiency of nonradiative quenching. For both systems studied here, the adsorption sites are not known. Even for much more extensively studied alkanethiol SAMs on Au(111), the structure of the molecule/substrate interface is still controversial both from an experimental<sup>55–57</sup> and a theoretical point of view.<sup>58–62</sup>

However, a recent STM<sup>63,64</sup> and high-resolution X-ray photoelectron spectroscopy study<sup>65</sup> for the BP $n$  series indicates that a modification of the intermolecular interaction by changing the parameter  $n$  from odd to even induces a change in the unit cell structure (i.e., from  $2\sqrt{3}\times 3$  to  $(5\sqrt{3}\times 3)$ rect, respectively) and in the adsorption sites of molecules. Since available STM data for BP2/Au(111)<sup>63</sup> and PEM/Au(111)<sup>66</sup> show different structures, a difference in the adsorption sites is very likely to occur also in this case.

In summary of the above discussion, we propose that differences in the Au–S–C bond angle and/or the adsorption sites affect the efficiency of nonradiative quenching and, therefore, electron-induced cleavage of the Au–S and S–C bonds for BP2 and PEM systems. In our opinion, this hypothesis is also supported by a recently reported odd–even effect in the electron-induced damage of BP $n$ /Au(111) systems,<sup>35</sup> where both differences in the Au–S–C bond angle and in the adsorption sites have been concluded from the previous spectroscopic<sup>43,65</sup> and very recent microscopic data.<sup>63,64</sup> Furthermore, since it is known that alkanethiols adsorb in  $sp^3$  and  $sp$  hybridization on Au(111) and Ag(111), respectively (and most probably have different adsorption sites), one could also expect differences in the electron-induced thiol–substrate bond scission in these two cases. Following this prediction, Zharnikov et al. have observed a strong difference in bond scission between Au–S and Ag–S in their electron irradiation experiments of alkanethiols deposited on Au and Ag substrates.<sup>34</sup>

The analysis of the electron-induced damage in BP2 and PEM (as shown in Figures 7 and 8) shows that the decrease in the photoion signal is similar in character to the electron-induced changes reported in XPS, NEXAFS, and IR investigations of alkanethiol monolayers.<sup>26,27,31,34</sup> Here, we have shown that this decrease results from at least two processes that lead to the degradation of the SAM: the gradual decomposition of the organic overlayer into a carbonaceous layer on the substrate and the direct desorption of intact molecules and molecular fragments from the layer. With only a limited number of data points available, a comparison of these results to a more specific kinetic rate law is not yet possible. However, the decay of the signals presented in Figures 7 and 8 may be described by a first-order exponential decay function given by the following expression:

$$D(Q) = D_{\text{SAT}} + (D_0 - D_{\text{SAT}}) \cdot \exp\left(-\frac{\sigma \cdot Q}{e \cdot S}\right) \quad (1)$$

where  $Q$  is the charge delivered to the surface,  $D_{\text{SAT}}$  and  $D_0$  correspond to the saturation and the initial value of the photoion signal,  $\sigma$  is the damage cross section,  $e$  is the charge of the electron, and  $S$  is the area irradiated by the electron beam. As a result, the following values of the cross sections were obtained:  $(2.9 \pm 0.6) \times 10^{-16} \text{ cm}^2$  for  $m/z = 78$ ,  $(4.9 \pm 0.7) \times 10^{-16} \text{ cm}^2$  for  $m/z = 104$ ,  $(3.7 \pm 1.3) \times 10^{-16} \text{ cm}^2$  for  $m/z = 194$ , and  $(9.4 \pm 2.0) \times 10^{-16} \text{ cm}^2$  for  $m/z = 228$ . Comparing data obtained for PEM and BP2 separately, it is clear that the electron-induced damage is higher for the higher mass of the analyzed fragment. In this case, two fragments are compared and the first one is a part of the second one (i.e.,  $m/z = 78$  is a part of  $m/z = 104$  and  $m/z = 194$  is a part of  $m/z = 228$ ). It can be expected that the larger fragment should exhibit a higher probability for electron-induced damage. The values obtained for these cross sections are comparable with those previously reported for damage of alkanethiols on Au(111) by low-energy electrons.<sup>27,34</sup> However, with our approach we do not determine the cross section for the damage (or modifica-

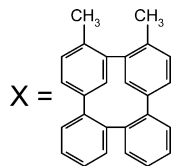


**Figure 12.** Schematic drawing of the molecule detected in positive SIMS spectra of BP0/Au presented in Figure 11 (h–o). See text for details.

tion) of a certain chemical bond<sup>27,34</sup> or the total thickness of the layer,<sup>34</sup> but we are able to analyze the cross section for the electron-induced damage of the intact molecule or specific fragment and thus gain complementary information.

Finally, we would like to comment on the SIMS experiment that is designed to probe chemical changes of the BP0/Au(111) system induced by electron irradiation followed by a long exposure to air. In agreement with the SIMS investigation made by Tarlov et al.<sup>49</sup> for alkanethiols on gold exposed to air for an extended period of time, these experiments show a progressive formation of sulfonate species. However, data presented here show that the signal intensity of these sulfonate species decreases as a function of the total electron fluence during sample irradiation prior to the air exposure. Thus, it shows that electron irradiation increases the stability of the system as was concluded from chemical etching experiments.<sup>32</sup> In addition, our experiments show a decrease of the characteristic secondary ions in both negative and positive spectra as a function of electron fluence. However, after high-fluence irradiation, two new peaks at  $m/z = 331$  and  $332$  are observed in the positive spectra. It can be assumed that the peak at  $m/z = 331$  corresponds to the  $(X-H)^+$  secondary ion, where X is a molecule schematically presented in Figure 12. Most probably, for the creation of such a molecule during electron irradiation, two neighboring BP0 molecules must form two bonds between their phenyl rings after earlier loss of hydrogen atoms (see Figure 11). Such an interpretation of the peak observed at  $m/z = 331$  is supported by the presence of a smaller peak at  $m/z = 332$ . The measured intensity ratio of the  $332/331$  peaks is  $0.27 \pm 0.02$ , which is within the accuracy of the measurement equal to a value of 0.28 as calculated from the isotopic abundance for a  $X-H$  molecule. To the best of our knowledge, the disappearance of characteristic ions for irradiated samples and the simultaneous appearance of  $(X-H)^-$  secondary ion are the first direct evidences of a quasi-polymerization process. This process has up to now been assumed by others from indirect observations for similar aromatic SAM systems.<sup>32,35,67</sup>

**Ion Irradiation Experiments.** Considering the decrease of the signal in Figure 4 for the total ion fluence of  $3.75 \times 10^{12}$  ions/cm<sup>2</sup>, and assuming the density of molecules obtained from STM experiments ( $3.7 \times 10^{14}$  molecules/cm<sup>2</sup> for BP2<sup>63</sup> and  $3.5 \times 10^{14}$  molecules/cm<sup>2</sup> for PEM<sup>66</sup>), we can very roughly approximate that on average the impact of a single 15 keV Ar<sup>+</sup> ion will modify about 70 BP2 and 30 PEM molecules. High efficiency of ion-induced modification of SAMs is consistent with previous desorption experiments for PEM/Au<sup>36,37</sup> and BP2/Au<sup>38</sup> monolayers. The majority of molecules desorbed by ion impact are emitted with low (thermal) energies. This observation was explained by a chemical reaction model and the contribution of secondary electrons that gently break the chemical bonds.<sup>36–38</sup> Computer simulations show that many of the surface molecules near the primary ion impact zone are severely damaged and yield reactive species such as H•, as well as other ionic and neutral fragments.<sup>68,69</sup> These unstable species can react with intact molecules and sever the chemical bonds. Bond scission

by chemical reaction is more gentle than direct bond scission by ion impact and is more likely to form products which may be trapped at the surface and finally evaporate with low kinetic energies.<sup>36–38</sup> Since these reaction fragments formed during ion impact can penetrate far away from the ion impact point, the area from where the molecules can desorb is larger than the surface area influenced by the collision cascade that develops in the substrate. This observation could properly account for a high-ion-induced damaged cross section as demonstrated in the present contribution. In addition, ion bombardment is associated with the emission of low-energy electrons. Therefore, such a process could also contribute to molecular desorption.

In the present study (as shown in Figure 4), we observed that after irradiation with a total ion fluence of  $3.7 \times 10^{12}$  ions/cm<sup>2</sup>, the signal of the desorbed neutral molecular fragment at  $m/z = 194$  decreases by about 70% for BP2. Our electron desorption experiments presented in the previous section show that, to observe the same range of signal decrease, one needs a total fluence of  $6.2 \times 10^{15}$  electrons/cm<sup>2</sup> with 150 eV energy. As a consequence, the assumption that bond breaking by secondary electrons is the sole process leading to molecular desorption requires a secondary electron yield of several thousand. Such a high value is rather improbable. For example, for a clean polycrystalline gold sample irradiated by 8 keV Ar<sup>+</sup>, the secondary electron yield was 0.34.<sup>70</sup> We are not aware of any measurements of secondary electron yields for ion-irradiated SAMs, but we may consider measurements made by Szapiro et al. for graphite bombarded by 8 keV Ar<sup>+</sup> which showed a secondary electron yield of about 2.<sup>71</sup> Therefore, we conclude that secondary electrons will not contribute predominantly to the damage induced by ion irradiation, but that the contribution of this mechanism cannot be ignored, either.

Desorption experiments for BP2 monolayers show that ion-induced processes may lead to the cleavage of both Au–S and S–C bonds. Results obtained for PEM indicate that cleavage of the Au–S bond is much less effective in comparison to the S–C bond scission. Taking into account the similar chemical composition of both BP2 and PEM monolayers, such a difference in ion-induced desorption is very intriguing in our opinion. Significant differences in the thiolate–substrate ion-induced bond scission have already been reported by Chenakin et al. for alkanethiols monolayers prepared on Au and Ag substrates.<sup>72</sup> The authors propose that a much higher desorption cross section of sulfur species from the alkanethiol/Au sample can be explained by a lower strength of the Au–S bond as compared to Ag–S. However, our results obtained for BP2/Au and PEM/Au cannot be explained in this way because these systems are very similar. Therefore, a different approach is needed. Assuming that ion-induced chemical reactions lead to the gentle breaking of chemical bonds in PEM and BP2,<sup>36–38</sup> one has to consider that the cross section for any chemical reaction should depend on the detailed electronic structure of the reagents. If this were the case, one could assume that hybridization and adsorption sites may influence this cross section and thus may be responsible for the observed differences in the Au–S bond scission for BP2/Au and PEM/Au monolayers. In addition, as the sulfur hybridization of alkanethiols on Au and Ag substrates is different, this might have to be taken into consideration, to explain the results obtained by Chenakin et al.

Finally, we would like to mention that, to further examine our hypothesis about strong influence of the details of the metal–molecule interface (e.g., adsorption sites and Au–S–C angle) on electron- and ion-induced desorption of SAMs, more

direct experiments are planned. Namely, we will compare electron- and ion-induced desorption for the SAMs made from the same molecule but arranged in different densely packed structures. In fact, this became possible only very recently because of our experiments on BP<sub>n</sub> SAMs (including investigated here BP2), which demonstrates the possibility of creating different high-density SAM structures for the same molecule.<sup>73,74</sup> These experiments are currently in progress.

## V. Conclusions

To enhance the efficiency of ion and electron beam lithography with thiol-based SAM/Au systems, it is necessary to develop an effective method for dissociating the Au–S bond and completely removing the organic molecules. Results presented here for the PEM/Au and BP2/Au systems show that this process is very sensitive to the structure of the SAM molecules. A better understanding of this structure correlation could give us a route toward purposeful design of SAMs optimized for lithographic applications. As discussed in this article, the possible origin for the observed differences in Au–S scission is attributed to the differences in the orientation of the Au–S–C angle or adsorption sites of the molecules. The analysis of the ion-induced modification of PEM/Au and BP2/Au shows that this process is very efficient and interaction with the single ion leads to the modification of tens of molecules. This observation is consistent with a previously proposed model, in which desorption of the majority of molecules is not caused by ballistic processes but by the chemical reaction or secondary electrons initiated by the ion impact.

Comparison of the electron- and ion-induced damage indicates that secondary electrons do not contribute significantly to the damage induced by ion irradiation. The efficient ion-induced damage of SAMs has in our opinion two important consequences. First, it shows that to maintain static conditions of ion irradiation, the total ion fluence needs to be kept below 10<sup>11</sup> ions/cm<sup>2</sup>. Second, because tens of molecules can be modified by a single ion, it sets the limits of the minimal size of nanostructures created in these aromatic SAMs by ion lithography.

The in-situ analysis of the electron-irradiated PEM/Au and BP2/Au using ion-initiated laser probing enabled measurement of the cross section for the electron-induced damage of the intact molecule or specific fragment. Thus, it is possible to gain complementary information to that obtained with other experimental techniques, where cross sections for specific bond scissions or total film thicknesses are measured. The ex-situ analysis of the electron-irradiated BP0/Au system with TOF–SIMS yields direct evidence of the quasi-polymerization process. It is this process which makes aromatic SAMs useful as a positive electron beam resist and which has up to now been assumed by others from indirect observations.

**Acknowledgment.** We would like to thank Dr. Manfred Buck for supplying us with BP2 and BP0 molecules. This work was financially supported by the Belgian Fund for Scientific Research – Flanders (FWO), Flemish Concerted Action Research Program (GOA/2004/02), Interuniversity Poles of Attraction Program (IAP/P5/01) – Belgian State, Prime Minister's Office – Federal Office for Scientific, Technical, and Cultural Affairs, Polish Committee of Scientific Research program no. 3T09A12426, Polish-Flanders Scientific Collaboration Program. P.C. is a Postdoctoral fellow of the Alexander von Humboldt Foundation. E.V. is a Postdoctoral Fellow of the FWO.

## References and Notes

(1) Ulman, A. *Chem. Rev.* **1996**, *96*, 1533.

- (2) Stewart, K. R.; Whitesides, G. M.; Godfried, H. P.; Silvera, I. F. *Surf. Sci.* **1986**, *57*, 1381.
- (3) Lee, T. R.; Laibinis, P. E.; Folkers, J. P.; Whitesides, G. M. *Pure Appl. Chem.* **1991**, *63*, 821.
- (4) Hild, R.; David, C.; Müller, H. U.; Völkel, B.; Kayser, D. R.; Grunze, M. *Langmuir* **1998**, *14*, 342.
- (5) Ulman, A. *J. Mater. Ed.* **1989**, *11*, 205.
- (6) Sagiv, J. *J. Am. Chem. Soc.* **1980**, *102*, 92.
- (7) Sheen, C. W.; Shi, J.-X.; Martensson, J.; Parikh, A. N.; Allara, D. L. *J. Am. Chem. Soc.* **1992**, *114*, 1514.
- (8) Laibinis, P. E.; Nuzzo, R. G.; Whitesides, G. M. *J. Phys. Chem.* **1992**, *96*, 5097.
- (9) Joyce, S. A.; Thomas, R. C.; Houston, J. E.; Michalske, T. A.; Crooks, R. M. *Phys. Rev. Lett.* **1992**, *68*, 2790.
- (10) Laibinis, P. E.; Whitesides, G. M. *J. Am. Chem. Soc.* **1992**, *114*, 9022.
- (11) Li, C.; Zhang, D. H.; Liu, X. L.; Han, S.; Tang, T.; Zhou, C. W.; Fan, W.; Koehne, J.; Han, J.; Meyyappan, M.; Rawlett, A. M.; Price, D. W.; Tour, J. M. *Appl. Phys. Lett.* **2003**, *82*, 645.
- (12) Donhauser, Z. J.; Mantooh, B. A.; Kelly, K. F.; Bumm, L. A.; Monnell, J. D.; Stapleton, J. J.; Price, D. W.; Rawlett, A. M.; Allara, D. L.; Tour, J. M.; Weiss, P. S. *Science* **2001**, *292*, 2303.
- (13) Reed, M. A.; Chen, J.; Rawlett, A. M.; Price, D. W.; Tour, J. M. *Appl. Phys. Lett.* **2001**, *78*, 3735.
- (14) Tour, J. M.; Jones, L.; Pearson, D. L.; Lamba, J. J. S.; Burgin, T. P.; Whitesides, G. M.; Allara, D. L.; Parikh, A. N.; Atre, S. V. *J. Am. Chem. Soc.* **1995**, *117*, 9529.
- (15) Bumm, L. A.; Arnold, J. J.; Cygan, M. T.; Dunbar, T. D.; Burgin, T. P.; Jones, L.; Allara, D. L.; Tour, J. M.; Weiss, P. S. *Science* **1996**, *271*, 1705.
- (16) Ishida, T.; Mizutani, W.; Akiba, U.; Umemura, K.; Inoue, A.; Choi, N.; Fujihira, M.; Tokumoto, H. *J. Phys. Chem. B* **1999**, *103*, 1686.
- (17) Ishida, T.; Fukushima, H.; Mizutani, W.; Miyashita, S.; Ogiso, H.; Ozaki, K.; Tokumoto, H. *Langmuir* **2002**, *18*, 83.
- (18) Buckel, F.; Effenberger, F.; Yan, C.; Golzhauser, A.; Grunze, M. *Adv. Mater.* **2000**, *12*, 901.
- (19) Zehner, R. W.; Sita, L. R. *Langmuir* **1997**, *13*, 2973.
- (20) Lercel, M. J.; Craighead, H. G.; Parikh, A. N.; Seshardi, K.; Allara, D. L. *Appl. Phys. Lett.* **1996**, *68*, 1504.
- (21) Lercel, M. J.; Whelan, C. S.; Craighead, H. G.; Seshardi, K.; Allara, D. L. *J. Vac. Sci. Technol., B* **1996**, *14*, 4085.
- (22) Ada, E. T.; Hanley, L.; Etchin, S.; Melngailis, J.; Dressick, W. J.; Chen, M. S.; Calvert, J. M. *J. Vac. Sci. Technol., B* **1995**, *13*, 2189.
- (23) Sun, S. Q.; Chong, K. S. L.; Leggett, G. J. *J. Am. Chem. Soc.* **2002**, *124*, 2414.
- (24) Götzhäuser, A.; Geyer, W.; Stadler, V.; Eck, W.; Grunze, M. *J. Vac. Sci. Technol., B* **2000**, *18*, 3414.
- (25) Felgenhauer, T.; Yan, C.; Geyer, W.; Rong, H.-T.; Götzhäuser, A.; Buck, M. *Appl. Phys. Lett.* **2001**, *79*, 3323.
- (26) Seshadri, K.; Froyd, K.; Parikh, A. N.; Allara, D. L.; Lercel, M. J.; Craighead, H. G. *J. Phys. Chem.* **1996**, *100*, 15900.
- (27) Olsen, C.; Rowntree, P. A. *J. Chem. Phys.* **1998**, *108*, 3750.
- (28) Müller, H. U.; Zharnikov, M.; Völkel, B.; Schertel, A.; Harder, P.; Grunze, M. *J. Phys. Chem. B* **1998**, *102*, 7959.
- (29) Kondoh, H.; Nozoye, H. *J. Phys. Chem. B* **1998**, *102*, 2367.
- (30) Rading, D.; Kesting, R.; Benninghoven, A. *J. Vac. Sci. Technol., A* **1998**, *16*, 3449.
- (31) Zharnikov, M.; Geyer, W.; Götzhäuser, A.; Frey, S.; Grunze, M. *Phys. Chem. Chem. Phys.* **1999**, *1*, 3163.
- (32) Geyer, W.; Stadler, V.; Eck, W.; Zharnikov, M.; Götzhäuser, A.; Grunze, M. *Appl. Phys. Lett.* **1999**, *75*, 2401.
- (33) Hutt, D. A.; Leggett, G. J. *J. Mater. Chem.* **1999**, *9*, 923.
- (34) Zharnikov, M.; Frey, S.; Heister, K.; Grunze, M. *Langmuir* **2000**, *16*, 2697.
- (35) Frey, S.; Rong, H.-T.; Heister, K.; Yang, Y.-J.; Buck, M.; Zharnikov, M. *Langmuir* **2002**, *18*, 3142.
- (36) Riederer, D. E.; Chatterjee, R.; Rosencrance, S. W.; Postawa, Z.; Dunbar, T. D.; Allara, D. L.; Winograd, N. *J. Am. Chem. Soc.* **1997**, *119*, 8089.
- (37) Cyganik, P.; Postawa, Z.; Meserole, C. A.; Vandeweert, E.; Winograd, N. *Nucl. Instrum. Methods Phys. Res., Sect. B* **1999**, *148*, 137.
- (38) Postawa, Z.; Meserole, C. A.; Cyganik, P.; Szymonska, J.; Winograd, N. *Nucl. Instrum. Methods Phys. Res., Sect. B* **2001**, *182*, 148.
- (39) Rowntree, P.; Dugal, P. C.; Hunting, D.; Sanche, L. *J. Phys. Chem.* **1996**, *100*, 4546.
- (40) Huels, M. A.; Dugal, P. C.; Sanche, L. *J. Phys. Chem.* **2003**, *118*, 11168.
- (41) Vandeweert, E.; Bastiaansen, J.; Vervaecke, F.; Lievens, P.; Silverans, R. E.; Cyganik, P.; Postawa, Z.; Rong, H.-T.; Buck, M. *Appl. Phys. Lett.* **2003**, *82*, 1114.
- (42) Vandamme, N.; Verschoren, G.; Depuydt, A.; Cannaearts, M.; Bouwen, W.; Lievens, P.; Silverans, R. E.; Van Haesendonck, C. *Appl. Phys. A* **2001**, *72*, S177.

- (43) Rong, H. T.; Frey, S.; Yang, Y. J.; Zharnikov, M.; Buck, M.; Wühh, W.; Wöll, C.; Helmchen, G. *Langmuir* **2001**, *17*, 1582.
- (44) Vandeweert, E.; Lievens, P.; Philipsen, V.; Bastiaansen, J.; Silverans, R. E. *Phys. Rev. B* **2001**, *64*, 195417.
- (45) Vandeweert, E.; Meserole, C. A.; Sosteracz, A.; Dou, Y.; Winograd, N.; Postawa, Z. *Nucl. Instrum. Methods Phys. Res., Sect. B* **2000**, *164–165*, 820.
- (46) Braun, R. M.; Blenkinsopp, P.; Mullock, S. J.; Corlett, C.; Willey, F.; Vickerman, J. C.; Winograd, N. *Rapid Commun. Mass Spectrom.* **1998**, *12*, 1246.
- (47) We assume that the emission of the intact BP2 molecule results from the recombination of desorbed thiolate molecule with the hydrogen which is released during irradiation by cleavage of the C–H bonds.
- (48) Frisbi, C. D.; Martin, J. R.; Duff, R. R.; Wighton, M. S. *J. Am. Chem. Soc.* **1992**, *114*, 7142.
- (49) Tarlov, M. J.; Newman, J. G. *Langmuir* **1992**, *8*, 1398.
- (50) Rading, D.; Kersting, R.; Benninghoven, A. *J. Vac. Sci. Technol., A* **2000**, *18*, 312.
- (51) Avouris, P.; Persson, B. N. J. *J. Phys. Chem.* **1984**, *88*, 837.
- (52) Sellers, H.; Ulman, A.; Shnidman, Y.; Eilers, J. E. *J. Am. Chem. Soc.* **1993**, *115*, 9389.
- (53) Tao, Y. -T.; Wu, C. C.; Eu, J. Y.; Lin, W. L.; Wu, K. C.; Chen, C. H. *Langmuir* **1997**, *13*, 4018.
- (54) Bratkowsky, A. M.; Kornilovitch, P. E. *Phys. Rev. B* **2003**, *67*, 115307.
- (55) Kondoh, H.; Iwasaki, M.; Shimida, T.; Amemiya, K.; Yokoyama, T.; Ohta, T.; Shimomura, M.; Kono, S. *Phys. Rev. Lett.* **2003**, *90*, 066102.
- (56) Fenter, A.; Eberhardt, A.; Eisenberger, P. *Science* **1994**, *266*, 1216.
- (57) Kluth, G. J.; Carraro, C.; Maboudian, R. *Phys. Rev. B* **1999**, *59*, 10449.
- (58) Beardmore, K. M.; Kress, J. D.; Gronbeck-Jensen, N.; Bishop, A. R. *Chem. Phys. Lett.* **1998**, *40*, 286.
- (59) Yourdshahyan, Y.; Zhang, H. K.; Rappe, A. M. *Phys. Rev. B* **2001**, *63*, 081405.
- (60) Gottschalck J.; Hammer B. *J. Chem. Phys.* **2002**, *116*, 784.
- (61) Hayashi, T.; Morikawa, Y.; Nozoye, H. *J. Chem. Phys.* **2001**, *114*, 7615.
- (62) Franzen, S. *Chem. Phys. Lett.* **2003**, *381*, 315.
- (63) Cyganik, P.; Buck, M.; Azzam, W.; Wöll, Ch. *J. Phys. Chem. B* **2004**, *108*, 4989.
- (64) Azzam, W.; Cyganik, P.; Witte, G.; Buck, M.; Wöll, Ch. *Langmuir* **2003**, *19*, 8262.
- (65) Heistler, K.; Rong, H. T.; Buck, M.; Zharnikov, M.; Grunze, M.; Johansson, L. S. O. *J. Phys. Chem. B* **2001**, *105*, 6888.
- (66) Because PEM/Au(111) structures reported in ref 37 and recently by Yang et al. (Yang, G.; Liu, G.-Y. *J. Phys. Chem. B* **2003**, *107*, 8746) are very different, i.e.,  $(\sqrt{3} \times \sqrt{3})R30^\circ$  ( $21.6 \text{ \AA}^2/\text{molecule}$ ) and  $7 \times \sqrt{3}$  ( $50.4 \text{ \AA}^2/\text{molecule}$ ), respectively, we have performed more detailed STM investigations which show that the PEM/Au(111) structure is in fact  $4 \times \sqrt{3}$  ( $28.8 \text{ \AA}^2/\text{molecule}$ ). Details of this STM study will be published in a separate contribution.
- (67) Kuller, A.; Eck, W.; Stadler, V.; Geyer, W.; Gölzhäuser, A. *Appl. Phys. Lett.* **2003**, *82*, 3776.
- (68) Taylor, R. S.; Garrison, B. J. *Int. J. Mass. Spectrom.* **1995**, *143*, 225.
- (69) Chatterjee, R.; Postawa, Z.; Winograd, N.; Garrison, B. J. *J. Phys. Chem. B* **1999**, *103*, 151.
- (70) Zalm, P. C.; Beckers, L. J. *Philips J. Res.* **1984**, *39*, 61.
- (71) Szapiro, B.; Rocca, J. J. *J. Appl. Phys.* **1989**, *65*, 3713.
- (72) Chenakin, S. P.; Heinz, B.; Morgner, H. *Surf. Sci.* **1999**, *421*, 337.
- (73) Cyganik, P.; Buck, M. *J. Am. Chem. Soc.* **2004**, *126*, 5960.
- (74) Cyganik, P.; Strunskus, T.; Shaporenko, A.; Wilton-Ely, J. D.; Buck, M.; Zharnikov, M.; Wöll, C., in preparation.